Supplementary Material for "Orbital-free density functional theory simulation of collective dynamics coupling in liquid Sn"

Beatriz G. del Rio,[1,2] **Mohan Chen**,[3] **Luis E. González**,[1] **and Emily A. Carter**[4]

[1]Departamento de Física Teórica, Atómica y Óptica, Universidad de Valladolid, 47011 Valladolid, Spain

[2]Department of Mechanical and Aerospace Engineering, Princeton University, Princeton, New Jersey 08544-5263, USA

[3]Department of Physics, Temple University, Philadelphia, Pennsylvania 19122, USA

[4]School of Engineering and Applied Science, Princeton University, Princeton, New Jersey 08544-5263, USA

S1. Sn LPS construction

The method used to construct the Sn local pseudopotential (LPS) followed two steps: 1) we constructed a Sn bulk-derived local pseudopotential (BLPS);[1] and 2) we modified the resulting BLPS by using a force-matching (FM)[2] process to better capture the liquid dynamics. The BLPS was constructed following the method previously introduced by Zhou *et al.*,[1] where converged valence electron densities from various crystalline phase structures of Sn, calculated with Kohn-Sham (KS) density functional theory (DFT) with a nonlocal pseudopotential (NLPS), were used as input to invert the KSDFT equations. A local KS effective potential is obtained from each valence electron density used as input. Afterwards, these effective potentials are unscreened by removing the Hartree electron repulsion and exchange-correlation (XC) potentials in order to obtain the approximate ionic external potential. As a consequence of using as a reference system a bulk crystalline environment, the atom-centered ionic potential (*i.e.*, the atomic BLPS) is obtained by using the bulk crystal's structure factor. Normally, all of these local potentials lie on a universal

curve, and a final BLPS can be obtained by the interpolation between all of the discrete data gathered for these atomic-centered ionic potentials. However, two free parameters are left to be tuned:[3] 1) the value of the non-Coulombic part of the BLPS in reciprocal space at q=0, namely $v_{nc}^{BLPS}(q = 0)$; and 2) r_c as the point beyond which the Coulombic tail is enforced onto the BLPS in real space, namely $v^{BLPS}(r)$. These two parameters, $v_{nc}^{BLPS}(q = 0)$ and r_c, are fit to reproduce the bulk moduli, equilibrium volumes, and relative phase energies obtained using an NLPS within KSDFT.

KSDFT calculations were performed using the ABINIT planewave (PW) DFT code.[4,5] We used a Troullier-Martins (TM) NLPS,[6] generated with the FHI98PP code[7] using the default core cutoff radii provided by the code. A Fermi-Dirac smearing with a width of 0.1 eV was used to smooth out the Fermi surface for all systems. All k-point meshes employed to sample the Brillouin zone were generated via the Monkhorst-Pack method.[8] Integration over the Brillouin zone is performed using a Fermi-Dirac smearing with a width of 0.1 eV for all systems. For the OFDFT calculations, although the Wang-Godvind-Carter99[9,10] kinetic energy density functional (KEDF) provided more accurate results for the solid phases, it exhibited divergence problems for *l*-Sn. We therefore used the Wang-Teter-style KEDF[11] with $\alpha = \beta = 1/2$, as parameterized by Smargiassi and Madden.[12]

For the BLPS construction, we used the KSDFT-NLPS reference valence electron densities and properties from the following crystalline structures: β-Sn, α-Sn, simple cubic (sc), face-centered cubic (fcc), and body-centered cubic (bcc). β- and α-Sn crystal structures are characterized by a tetragonal structure and a cubic structure, respectively. For geometry relaxations and energy calculations, we used the primitive cells consisting of two atoms for both β- and α-Sn, and one atom each for the sc, fcc, and bcc structures. The Monkhorst-Pack *k*-point grids employed for these cells were 20 x 20 x 35 and 15 x 15 x 15 for β- and α-Sn, respectively, and 20 x 20 x 20 for sc, fcc, and bcc. A 1200-eV kinetic-energy cutoff for the PW basis set was used. The selected PW kinetic energy cutoff and *k*-point meshes ensure that the accuracy of the total energy is converged to within

1.0 meV/atom. Convergence thresholds for the stress tensor elements and forces on ions were 5×10^{-7} hartree bohr^{-3} and 5×10^{-5} hartree bohr^{-1}, respectively.

The general representation of the *l*-Sn phases with OFDFT-BLPS fails, however, by predicting a melting point for Sn 50% higher than the experimental value.[13] We therefore used the FM method to improve the liquid representation; the FM method has been applied successfully to obtain accurate LPSs for liquid beryllium (Be), calcium (Ca), and barium (Ba).[2] The procedure starts by performing a KSDFT-NLPS molecular dynamics (MD) simulation (within either the NVT or NVE ensemble) of the liquid on a small sample over a short simulation time. The forces acting on each atom, which are obtained for each configuration of the KSDFT-MD/NLPS simulation, affect all of the liquid phase properties; a better representation of the forces implies a better representation of the liquid. Therefore, in the second step of the FM-BLPS construction, we randomly selected several atomic configurations from the KSDFT-MD/NLPS run and computed the forces acting on the atoms with OFDFT and the BLPS. Afterwards, the difference between OFDFT and KSDFT forces was minimized by modifying the BLPS through the addition of Gaussian functions in which the amplitudes and widths of each Gaussian are taken as fitting parameters. In this work, we used two Gaussians located at two regions in reciprocal space: $q = 0$ and $q = 2k_F$, where k_F is the Fermi momentum corresponding to the mean electron density of the system. The addition of the Gaussians is performed on the non-Coulombic part of the BLPS in reciprocal space. The benchmark KSDFT-MD/NLPS data used for the forces comparison was kindly provided by Calderín *et al.*[14] from their previous work on the evaluation of *l*-Sn's properties where they used 205 atoms. They also used the local density approximation (LDA) XC potential in their simulation as we do here.

The comparison between the initial BLPS and the final FM-BLPS is displayed in Figure S1. The main modification to the initial BLPS appears at $q = 0$, where the value of the BLPS is significantly lowered.

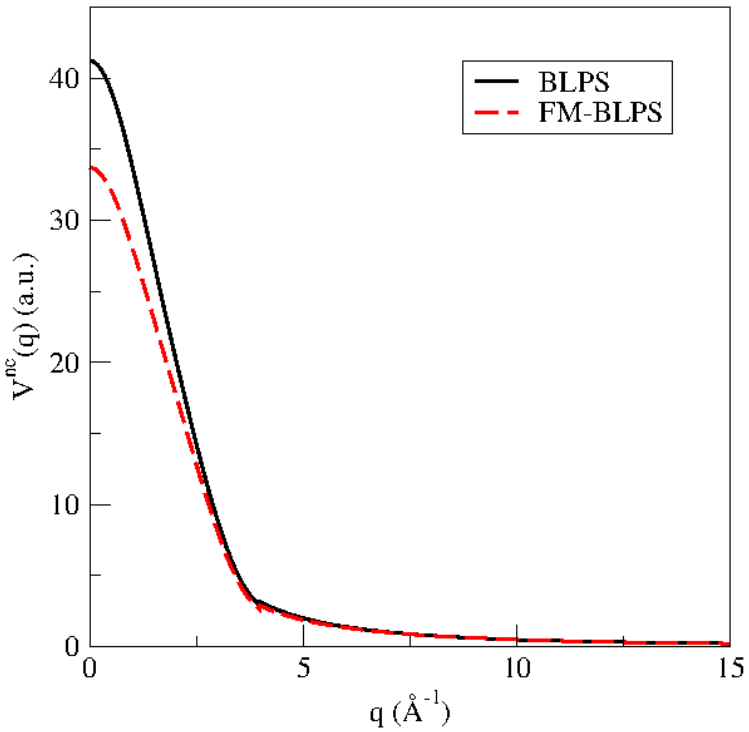

FIG S1. Non-Coulombic parts of the initial BLPS (solid line) and final FM-BLPS (dashed line).

We then calculated the melting temperature with both BLPS and FM-BLPS to evaluate the level of improvement obtained by including FM to refine the initial BLPS. We employed the Z-method[15,16] to eliminate the superheating that occurs in the heat-until-melts method and to avoid the extensive computational effort of liquid-solid coexistence simulations.[17–19] The Z-method is based on calculating the threshold of thermal stability where if a solid configuration is provided with higher energy than the liquid phase, then the system will melt and its temperature will drop to the melting temperature. The procedure only requires MD simulations run in the NVE ensemble. For each volume, various simulations are run, each with a different input energy determined by the input temperature. The systems used in this study contained 512 atoms in a β-Sn structure with a volume ranging from 0.042 Å^{-3} to 0.040 Å^{-3} in increments of 0.0005 Å^{-3}. The initial temperatures tested for each volume varied from 400 to 1200 K in increments of 100 K. The melting temperature obtained for the initial BLPS is 758 K, 253 K higher than the experimental value of 505 K.[13] The

melting temperature obtained with the FM-BLPS is 522 K, much closer to experimental value. Thus, by applying FM to the initial BLPS, we adapted the pseudopotential to more accurately represent the liquid phase.

S2. Thermodynamic, structural, and transport properties of l-Sn

The theoretical atomic densities for *l*-Sn at each different temperature were obtained with NPT OFDFT-MD simulations of 512-atom systems initially in a β-Sn structure (Table S.I).

TABLE S.I. Calculated atomic densities ($\rho_{\mathrm{OFDFT-MD}}$) and experimental atomic densities[20] (ρ_{exp}) for *l*-Sn at temperatures ranging from 573 to 1873 K.

T (K)	**573**	**673**	**773**	**873**	**973**	**1073**	**1273**	**1873**
$\boldsymbol{\rho_{\mathrm{OFDFT-MD}}}$	0.0411	0.0399	0.0394	0.0390	0.0386	0.0381	0.0375	0.0351
$\boldsymbol{\rho_{\mathrm{exp}}}$	0.0352	---	---	---	0.0337	0.0335	0.0325	0.0309

The computed atomic densities ($\rho_{\mathrm{OFDFT-MD}}$) are higher than the experimental values (ρ_{exp}). This increase in density is partly due to the use of the LDA XC functional, which overbinds atoms, producing too-small chemical bonds and hence cell volumes. To determine how the too-high density affects *l*-Sn, we evaluated different static and dynamic properties at each temperature and compared them to available experimental and computational data. The final systems used to compute all of the properties were composed of 1000 atoms. The cell volumes were defined by the atomic densities in Table S.I.

Static structure factor

An experimentally accessible quantity closely related to the atomic structure of the liquid is the static structure factor, $S(q)$, defined by the autocorrelation function,

$$S(q) = \frac{1}{N}\langle \rho(\vec{q})\rho(-\vec{q})\rangle, \quad (2)$$

where averages are taken over the wave vectors with the same magnitude and over configurations. In Figure S2, we compare predicted $S(q)$ for different temperatures along with the X-ray diffraction

data (XRD) of Waseda[20] and the inelastic neutron scattering (INS) of Itami *et al.*[21] The OFDFT-MD S(q) has a main peak that shifts negligibly with temperature, from $q_p \approx 2.38\ \text{Å}^{-1}$ at T= 573 K to $q_p \approx 2.34\ \text{Å}^{-1}$ at T= 1873 K. The second peak's position shifts equally little, from $\approx 4.58\ \text{Å}^{-1}$ at T= 573 K to $\approx 4.61\ \text{Å}^{-1}$ at T= 1873 K. The subsequent oscillations are rather weak for all temperatures. Some discrepancies with the experimental data are visible at the lower temperatures between 573 and 973 K, especially for the position of the main and second peaks. However, OFDFT-MD recovers correctly the height and amplitudes of the main and second peaks. Moreover, the shoulder on the high-*q* side of the main peak, which is the most distinctive feature of the measured S(q) for *l*-Sn, is also reproduced by OFDFT-MD at all of the temperatures studied.

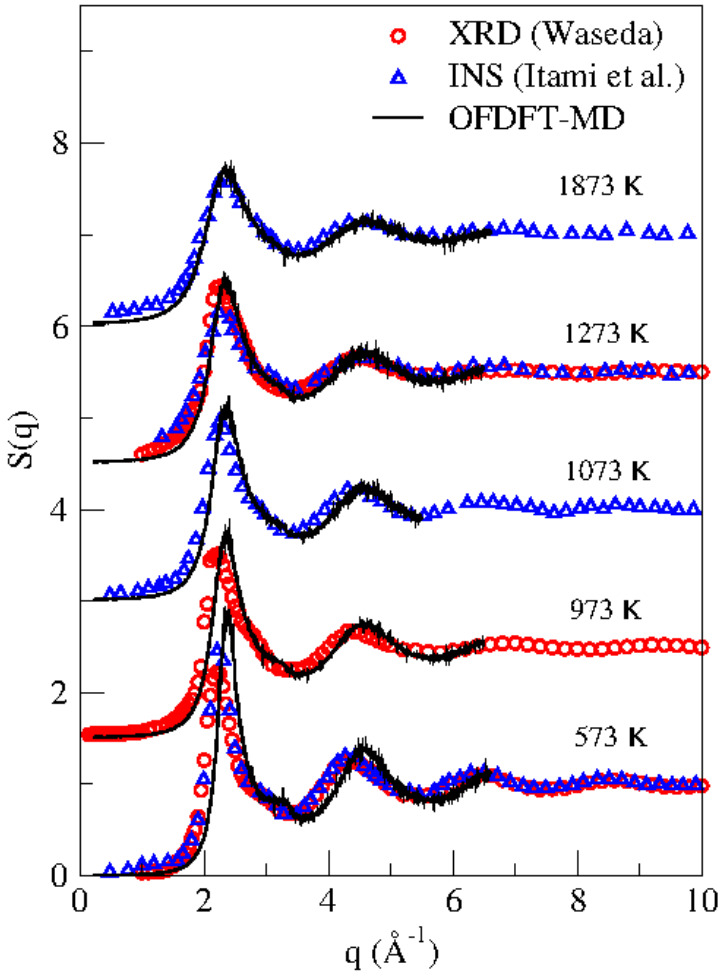

FIG. S2. Static structure factors of *l*-Sn at different temperatures from OFDFT-MD, along with experimental data of Waseda[20] and Itami *et al.*[21]

Self-diffusion coefficient

The self-diffusion coefficient can be obtained from the time integral of the velocity autocorrelation function, Z(t),[22]

$$D = \frac{1}{\beta m}\int Z(t)dt, \tag{3}$$

where m is the atomic mass, $\beta = {}^{1}/_{k_B T}$, k_B is the Boltzmann constant, and T is the temperature. We performed correlations on sets of 500 configurations for the calculation of Z(t).

Figure S3 displays the temperature dependence of the mean self-diffusion of Sn atoms in *l*-Sn at different temperatures. Comparison is provided with previous experiments and simulations, which exhibit significant dispersion in their results. Nevertheless, OFDFT-MD results follow the overall trend established by previous data. Specifically, OFDFT-MD results are slightly higher than Itami *et al.*'s KSDFT-MD data,[21] which simulated 64 atoms, but lower than Vella *et al.*'s[23] and Mouas *et al.*'s[24] classical (C)MD data, which simulated 5000 and 8000 atoms, respectively. This behavior suggests a clear dependence of the self-diffusion coefficient on the sample size, as previously studied by Yeh and Hummer.[25] They provided an expression to correct this shortcoming,

$$D_{corr} = D_{OFDFT-MD} + \frac{k_B T \xi}{6\pi\eta L}, \tag{5}$$

where k_B is the Boltzmann constant, T is the temperature, ξ is a constant equal to 2.837297, η is the OFDFT-MD viscosity, and L is the periodic cell length (assuming a cubic box). In Figure S3, the corrected values for the self-diffusion coefficient (OFDFT-MD corr.) for temperatures higher than 773 K closely follow those of CMD by Mouas *et al.* All of the simulations yield diffusivities

smaller than experiment, especially at high temperatures. However, the largest deviation is only a factor of two, which is acceptable.

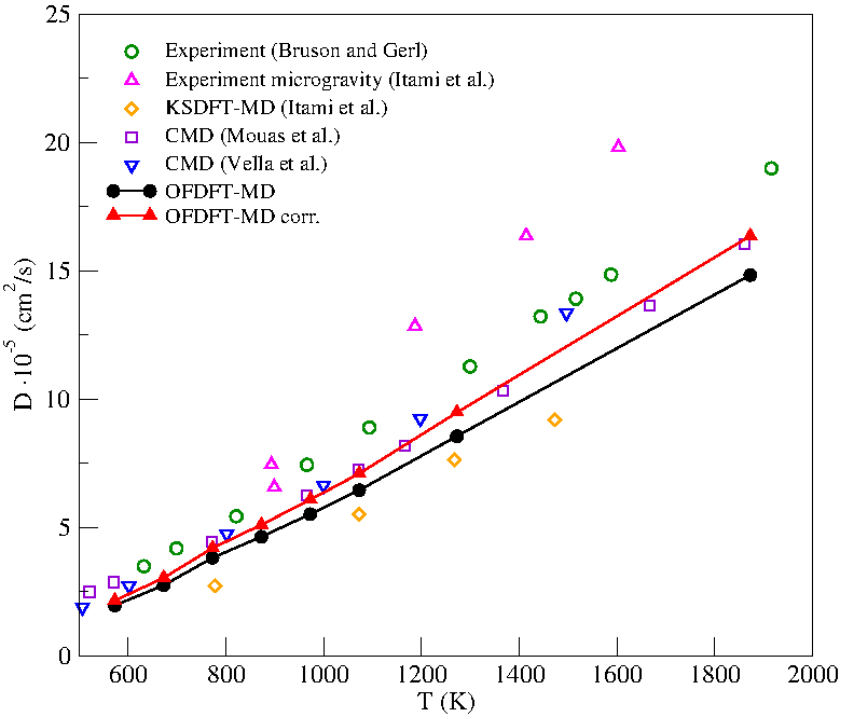

FIG. S3. Self-diffusion coefficients of *l*-Sn at different temperatures from OFDFT-MD, along with experimental and other MD data. Experimental data are taken from Bruson and Gerl[26] and Itami *et al.*[27] KSDFT-MD data are from Itami *et al.*,[21] and CMD data are from Mouas *et al.*[24] and Vella *et al.*[23] The error bars, representing a 95% confidence interval, are smaller than the symbols.

Chen *et al.*[28] studied in detail size effects on *l*-Li properties by performing both OFDFT-MD and CMD. They used cell sizes ranging from 250 to 1024 atoms for OFDFT-MD and from 250 to 6750 atoms for CMD. The self-diffusion coefficient curve obtained for the different cell sizes simulated at the same temperature was extrapolated to infinite cell sizes. They found that the correction parameter introduced by Yeh and Hummer[25] recovered the same values as the extrapolation procedure.

Adiabatic sound velocity

The dynamic structure factor, $S(q, \omega)$, at every temperature studied exhibits side peaks in a given wave-vector range, indicative of collective density excitations. The dispersion relation of such side peaks gives rise to a curve, $\omega_m(q)$, where the slope at $q \to 0$ equals the adiabatic sound velocity, c_s.[22] Figure S4 illustrates the temperature dependence of c_s and its comparison with previous measurements by Hosokawa *et al.*[29] and Blairs[30] as well as the analytical values obtained by the experimentally derived equation by Blairs.[30] Our OFDFT-MD results closely follow the experimental data, especially at temperatures lower than 1800 K; we therefore are able to correctly describe the collective density excitations present in the system.

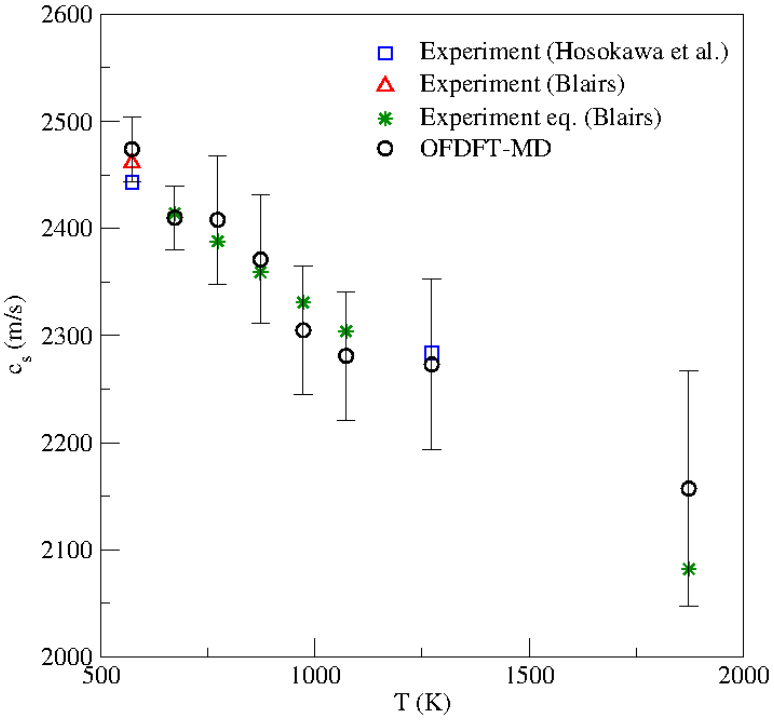

FIG. S4. Adiabatic sound velocities from OFDFT-MD and from experiments by Hosokawa *et al.*[29] and Blairs.[30] Stars: Predicted values from experimentally derived equation by Blairs.[30] The error bars represent a 95% confidence interval.

Shear viscosity coefficient

We calculated the shear viscosity *via* the transverse current correlation function, $C_T(q,\omega)$, by using the relationship,[22]

$$\eta(q) = \frac{k_B T \rho}{q^2 C_T(q,\omega=0)}, \tag{6}$$

where $\eta(q)$ is the generalized shear viscosity and ρ is the atomic density. The shear viscosity coefficient, η, is obtained by extrapolating $\eta(q)$ to $q \to 0$. For such an endeavor, we use a Lorentzian as introduced by Balucani *et al.*,[31]

$$\eta(q) = \frac{\eta}{1+aq^2}. \tag{7}$$

Results for the shear viscosity with respect to temperature for *l*-Sn are displayed in Figure S5. Along with our OFDFT-MD data, we include both experimental and CMD simulation data. As with the self-diffusion coefficient, the OFDFT-MD results are inside the region delimited by the experimental data, which exhibit a significant dispersion. Specifically, the OFDFT-MD results are close to the CMD results by Mouas *et al.*[24] and Vella *et al.*,[23] which fall into the intermediate region between the different experimental data sets.

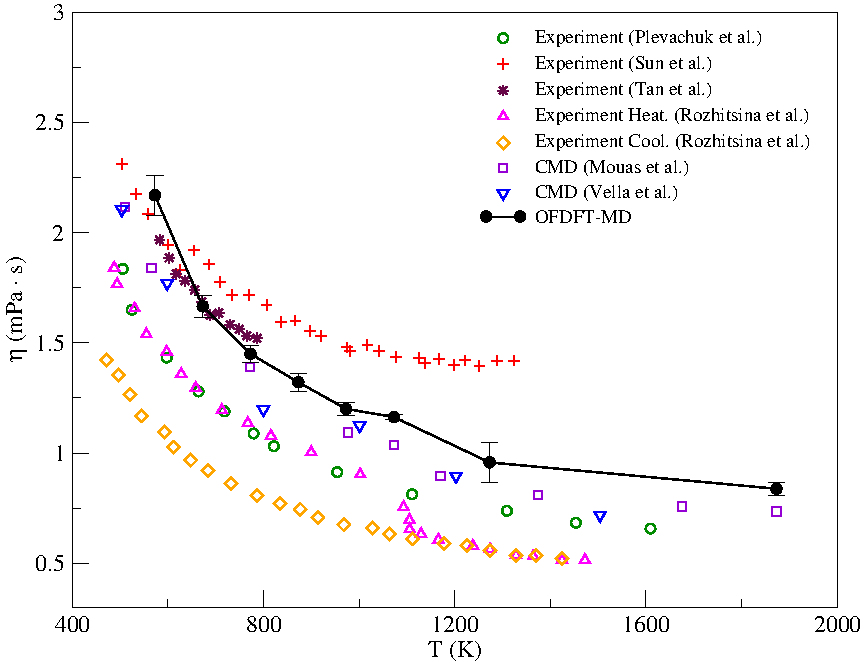

FIG. S5. Shear viscosities at different temperatures from OFDFT-MD, along with experimental and CMD data. Experimental data are from Plevachuk *et al.*,[32] Sun *et al.*,[33] Tan *et al.*,[34] and Rozhitsina *et al.* (following both a heating and cooling process).[35] CMD data are from Mouas *et al.*[24] and Vella *et al.*[23] The error bars represent a 95% confidence interval.

All of the studied properties agree quite well with available experimental data, suggesting that the overestimated atomic density does not significantly impact the results.

S3. Collective dynamics of *l*-Sn at 573 K

Intermediate scattering functions

Table S.II presents the different correlation sets used to evaluate the intermediate scattering functions $F(q,t)$. Time origins were taken at every time step. As the wave vector approaches the q_p value, the correlation sets increase in length because $F(q,t)$ decays more slowly in time, associated with the de-Gennes narrowing caused by strong structural correlations.[22]

TABLE S.II. Number of configurations used in the correlation sets for each wave-vector range in the evaluation of $F(q,t)$.

q-range (Å^{-1})						
0.216-0.375	0.433-0.650	0.685-1.877	2.068-2.242	2.355-2.471	2.672-3.066	3.230-4.670
2000	1000	700	2000	3000	2000	1200

Current correlation functions

Table S.III provides the different correlation sets and time origins used to evaluate both the transverse and longitudinal current correlation functions, $C_L(q,t)$ and $C_T(q,t)$. Time origins were always taken at every time step.

TABLE S.III. Number of configurations used in the correlation sets for each wave-vector range in the evaluation of $C_L(q,t)$ and $C_T(q,t)$.

q-range ($Å^{-1}$)		
0.216-0.375	0.433-0.650	0.685-4.670
2000	1200	700

REFERENCES

[1] B. Zhou, Y.A. Wang, and E.A. Carter, Phys. Rev. B **69**, 125109 (2004).

[2] B.G. del Rio and L.E. González, J. Phys. Condens. Matter **26**, 465102 (2014).

[3] C. Huang and E.A. Carter, Phys. Chem. Chem. Phys. **10**, 7109 (2008).

[4] X. Gonze, J.M. Beuken, R. Caracas, F. Detraux, M. Fuchs, G.M. Rignanese, L. Sindic, M. Verstraete, G. Zerah, F. Jollet, M. Torrent, A. Roy, M. Mikami, P. Ghosez, J.Y. Raty, and D.C. Allan, Comput. Mater. Sci. **25**, 478 (2002).

[5] X. Gonze, B. Amadon, P.M. Anglade, J.M. Beuken, F. Bottin, P. Boulanger, F. Bruneval, D. Caliste, R. Caracas, M. Côté, T. Deutsch, L. Genovese, P. Ghosez, M. Giantomassi, S. Goedecker, D.R. Hamann, P. Hermet, F. Jollet, G. Jomard, S. Leroux, M. Mancini, S. Mazevet, M.J.T. Oliveira, G. Onida, Y. Pouillon, T. Rangel, G.M. Rignanese, D. Sangalli, R. Shaltaf, M. Torrent, M.J. Verstraete, G. Zerah, and J.W. Zwanziger, Comput. Phys. Commun. **180**, 2582 (2009).

[6] N. Troullier and J.L. Martins, Phys. Rev. B **43**, 8861 (1991).

[7] M. Fuchs and M. Scheffler, Comput. Phys. Commun. **119**, 67 (1999).

[8] H.J. Monkhorst and J.D. Pack, Phys. Rev. B **13**, 5188 (1976).

[9] Y.A. Wang, N. Govind, and E.A. Carter, Phys. Rev. B **60**, 16350 (1999).

[10] Y.A. Wang, N. Govind, and E.A. Carter, Phys. Rev. B **64**, 89903 (2001).

[11] L.W. Wang and M.P. Teter, Phys. Rev. B **45**, 13196 (1992).

[12] E. Smargiassi and P.A. Madden, Phys. Rev. B **49**, 5220 (1994).

[13]*CRC Handbook of Chemistry and Physics* (CRC Press, Boca Raton, FL, 1977).

[14] L. Calderín, D.J. González, L.E. González, and J.M. López, J. Chem. Phys. **129**, 194506 (2008).

[15] A.B. Belonoshko, N. V. Skorodumova, A. Rosengren, and B. Johansson, Phys. Rev. B **73**, 1 (2006).

[16] A.B. Belonoshko and A. Rosengren, Phys. Rev. B **85**, 1 (2012).

[17] J.R. Morris, C.Z. Wang, K.M. Ho, and C.T. Chan, Phys. Rev. B **49**, 3109 (1994).

[18] D. Alfè, Phys. Rev. B **68**, 64423 (2003).

[19] E.R. Hernández, A. Rodriguez-Prieto, A. Bergara, and D. Alfè, Phys. Rev. Lett. **104**, 185701 (2010).

[20] Y. Waseda, *The Structure of Non-Crystalline Materials: Liquids and Amorphous Solids* (New York: McGraw-Hill International Book Co., 1980).

[21] T. Itami, S. Munejiri, T. Masaki, H. Aoki, Y. Ishii, T. Kamiyama, Y. Senda, F. Shimojo, and K. Hoshino, Phys. Rev. B **67**, 64201 (2003).

[22] U. Balucani and M. Zoppi, *Dynamics of the Liquid State* (Clarendon Press, Oxford, 1994).

[23] J.R. Vella, M. Chen, F.H. Stillinger, E.A. Carter, P.G. Debenedetti, and A.Z. Panagiotopoulos, Phys. Rev. B **95**, 1 (2017).

[24] M. Mouas, J.G. Gasser, S. Hellal, B. Grosdidier, A. Makradi, and S. Belouettar, J. Chem. Phys.

136, (2012).

[25] I.C. Yeh and G. Hummer, J. Phys. Chem. B **108**, 15873 (2004).

[26] A. Bruson and M. Gerl, Phys. Rev. B **21**, 5447 (1980).

[27] T. Itami, T. Masaki, H. Aoki, S. Munejiri, M. Uchida, S. Matsumoto, K. Kamiyama, and K. Hoshino, J. Non. Cryst. Solids **312**–**314**, 177 (2002).

[28] M. Chen, J.R. Vella, A.Z. Panagiotopoulos, P.G. Debenedetti, F.H. Stillinger, and E.A. Carter, AIChE J. **61**, 2841 (2015).

[29] S. Hosokawa, J. Greif, F. Demmel, and W.-C. Pilgrim, Chem. Phys. **292**, 253 (2003).

[30] S. Blairs, Int. Mater. Rev. **52**, 321 (2007).

[31] U. Balucani, J.P. Brodholt, P. Jedlovszky, and R. Vallauri, Phys. Rev. E **62**, 2971 (2000).

[32] Y. Plevachuk, V. Sklyarchuk, W. Hoyer, and I. Kaban, J. Mater. Sci. **41**, 4632 (2006).

[33] C. Sun, H. Geng, L. Ji, Y. Wang, and G. Wang, J. Appl. Phys. **102**, (2007).

[34] M. Tan, B. Xiufang, X. Xianying, Z. Yanning, G. Jing, and S. Baoan, Phys. B Condens. Matter **387**, 1 (2007).

[35] E. V. Rozhitsina, S. Gruner, I. Kaban, W. Hoyer, V.E. Sidorov, and P.S. Popel', Russ. Metall. **2011**, 118 (2011).